Proposal for making a beam of antihydrogen by two charge exchange events

F Robicheaux

Department of Physics, Auburn University, AL 36849-5311, USA

Abstract

We have performed calculations of two successive charge transfers in a geometry that could generate a beam of antihydrogen atoms ($\bar{H}$) or reliably produce cold $\bar{H}$ without having to reach extremely cold plasma temperatures. The basic idea is similar to that proposed by Hessels *et al* (1998 *Phys. Rev.* A **57** 1668) except that the order of the charge transfers is reversed. A beam of highly-excited (Rydberg) Cs atoms passes through an antiproton ($\bar{p}$) plasma where a charge transfer can take place; the result is an exotic Rydberg atom (Cs^+ ion and a bound $\bar{p}$) which has approximately the original velocity of the Cs atom since the Cs^+ mass is much greater than that of the $\bar{p}$. This exotic Rydberg atom travels into a positron plasma where a second charge exchange gives antihydrogen ($\bar{H}$). The velocity distribution of the resulting $\bar{H}$ is directly related to the original velocity of the Rydberg Cs atom. The binding energy of the $\bar{H}$ is roughly that of the original Cs Rydberg atom; thus, the starting state of the $\bar{H}$ can be controlled by choosing the initial state of the Cs atom. Because the $\bar{p}Cs^+$ binding energy can be controlled in the charge transfer, this first step, by itself, could be of interest to the exotic atom community.

1. Introduction

Experiments have demonstrated the formation of cold antihydrogen ($\bar{H}$) (e.g. see [1, 2]). Currently, there are two experimental collaborations, ALPHA (e.g. see [3]) and ATRAP, that are actively attempting to trap $\bar{H}$. In both collaborations, cold anti-protons, $\bar{p}$'s, traverse a cold positron, e^+, plasma; a $\bar{p}$ can capture one of the e^+'s during its brief time in the plasma. The plasmas are confined in the radial direction by a strong magnetic field and electric potential wells in the direction along the B-field. Presumably [4–6], the $\bar{H}$ is formed through three-body capture since this mechanism has the largest rate for the parameters of the experiments. In three-body capture, e^+'s scatter in the field of a $\bar{p}$ so that an e^+ loses enough energy to become bound to the $\bar{p}$. In both experimental apparati, the $\bar{p}$ start with a relatively large kinetic energy and slow down through their interaction with the e^+ plasma. The resulting $\bar{H}$'s have a broad velocity distribution; even if the $\bar{H}$ is cold, the direction of the velocity vector is random.

There have been a few proposals that could utilize a beam of $\bar{H}$. Also, it would be useful to explore different methods for generating $\bar{H}$ since the current method has troubles due to the preferential generation of hot $\bar{H}$. At this time, no one has successfully created an $\bar{H}$ beam although there are a few proposed schemes. For example, [7] proposes to use laser excited Ps to generate the $\bar{H}$ ($Ps^* + \bar{p} \rightarrow \bar{H} + e^-$) and an electric field gradient to accelerate the $\bar{H}$. Reference [8] proposes a trap utilizing magnetic quadrupole and electric octupole fields to simultaneously confine $\bar{p}$'s and e^+'s and the resulting $\bar{H}$ will be accelerated by the spatially varying fields. Reference [9] proposes to have $\bar{p}$'s pass through an e^+ plasma similar to [1, 2] but with a controlled speed for the $\bar{p}$'s so that when the recombination occurs the $\bar{H}$'s have a well-defined velocity. Reference [10] describes a method using a structured magnetic field from a series of parallel wires to generate an $\bar{H}$ beam. In this paper, I present simulations of a process that could be used to make an $\bar{H}$ beam. The method utilizes two separate charge transfers.

Reference [11] suggested that $\bar{H}$ could be made using a two-stage charge transfer to attach the e^+ to the $\bar{p}$. A beam of highly excited (Rydberg) atoms is directed through an e^+ plasma that is close to trapped $\bar{p}$'s. When the Rydberg atom enters the e^+ plasma, a charge exchange quickly occurs giving a highly excited positronium (Ps). A fraction of the Ps population travels to the region of the trapped $\bar{p}$'s where a second charge exchange can occur. The ATRAP collaboration
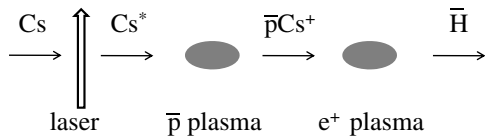
Figure 1. A schematic of the process considered in this paper. A Cs beam is directed towards the antimatter plasmas. The Cs is excited to a Rydberg state just before entering a $\bar{p}$ plasma. A charge exchange gives the exotic atom consisting of a Cs^+ ion and a bound $\bar{p}$ in a Rydberg state. This atom has essentially the same velocity as the original Cs atom. The exotic atom then enters a positron (e^+) plasma where a second charge exchange takes place which gives a $\bar{H}$ with the average velocity in the same direction as the original Cs atom.

reported a successful implementation [12] of this two-stage charge transfer method for $\bar{H}$ formation. Reference [13] presented calculations of this process in a strong B-field which showed that the basic process was unchanged by a strong magnetic field but that the B-field can substantially affect the final states by changing the distribution of magnetic moments of the $\bar{H}$.

In this paper, we present calculations of the two charge transfer processes but with the order of the transfers reversed from that in [11–13]. Figure 1 shows a schematic of this process. The idea is to have the Rydberg Cs atom (Cs^*) first pass through a $\bar{p}$ plasma. The Cs^* atom is assumed to have a velocity $\vec{V}_{Cs}$ along the B-field. The speed is assumed to be controllable and in a range of a few 100 m s^{-1} to ~1000 m s^{-1}. When the Cs^* atom is in the $\bar{p}$ plasma, a charge exchange can take place which can give an exotic Rydberg atom consisting of a Cs^+ ion and a bound $\bar{p}$: $\bar{p}Cs^+$. Due to velocity and size matching conditions during the charge transfer discussed below, the exotic Rydberg atom has a binding energy approximately equal to the binding energy of the Rydberg Cs atom, but reduced by the kinetic energy of the $\bar{p}$ in the frame of the Cs atom. Thus, by controlling the state of the original Rydberg atom, the state of the $\bar{p}Cs^+$ can be controlled to some extent as shown in section 3. Since the mass of the Cs is much greater than that of the $\bar{p}$, the velocity of the $\bar{p}Cs^+$ is approximately that of the original Cs atom. On average the velocity changes by less than 1%. Thus, the path of this exotic atom is well known.

In the second stage, the $\bar{p}Cs^+$ passes into a positron (e^+) plasma[1] where a second charge exchange can take place. When the second charge exchange gives a $\bar{H}$, the $\bar{H}$ also has a controllable average velocity in the frame of the Cs^+ ion. This means the $\bar{H}$ has an average velocity parallel to that of the original Cs atom because the relatively large ion mass means it is hardly deflected throughout this process. To summarize, this idea is based on the fact that the Cs mass is much greater than the $\bar{p}$ mass which is much greater than the e^+ mass.

This two-step process has some nice features. (1) The average $\bar{H}$ velocity is controlled through the velocity of the

original Cs atom. (2) The timing of the formation can be controlled by delivering the Cs Rydberg atoms in bunches. For example, by using a pulsed laser excitation to drive the Cs into a Rydberg state, the Rydberg atoms can be injected in pulses which could help in reducing background signal by using a time window on the detector. (3) The binding energy of the $\bar{H}$ is approximately that of the original Cs Rydberg atom because each charge exchange tends to preserve the size of the atom as discussed below and shown in figures 3 and 8. Thus, the binding energy of the $\bar{H}$ can be controlled by choosing which state of Cs to excite. (4) Neither the temperature of the $\bar{p}$ plasma nor that of the e^+ plasma is extraordinarily important. For example, the temperature of the positrons will weakly affect the probability for the second charge transfer but will hardly affect the kinetic energy of the resulting $\bar{H}$. (5) Finally, this method could provide a different mechanism for forming cold $\bar{H}$ even if the $\bar{H}$ velocity width is too large to be useful for some purposes. This can be done by sending in slow Cs so that the average velocity of the $\bar{H}$ is zero and the velocity spread depends predominately on the initial binding energy of the Cs atom.

Some of these features are also present in the original two-step process [11–13]. In particular, the timing (2) and binding energy (3) have similar properties to the original proposal. One advantage that the present method has over the original method is that there is little loss in going from the first to the second charge exchange. In the original method, there is a loss due to the fact that the positronium emerges isotropically which gives a decrease in $\bar{H}$ formation due to the small solid angle; the probability for the second charge transfer is $\sim N_{\bar{p}}\sigma_{cc}/(4\pi R^2)$, where $N_{\bar{p}}$ is the number of $\bar{p}$'s, $\sigma_{cc} \sim 10\pi a_0^2 n^4$ is the charge exchange cross section and R is the distance from the positrons to the $\bar{p}$'s (for example, 100 000 $\bar{p}$'s that are 3 cm away and a $\sigma_{cc} \sim 2 \times 10^{-9}$ cm^2 gives a probability for the second charge transfer of $\sim 10^{-6}$).

The process has one negative feature that seems impossible to remove and which may restrict its utility. The spread in the $\bar{H}$'s velocity distribution depends on the binding energy of the $\bar{p}Cs^+$. The velocity spread increases as the binding energy gets larger. By increasing the speed of the Rydberg atom, the spread becomes a smaller fraction of the average velocity. Unfortunately, the speed can only be increased up to a limit where the binding energy of the Rydberg atom is roughly equal to the kinetic energy of the $\bar{p}$ in the frame of the Cs atom. When the $\bar{p}$ speed is too large in the frame of the Cs atom, ionization of the Rydberg atom becomes the dominant process and the first charge exchange becomes negligible.

The main purpose of this paper is to present the result of calculations that give the limitations of the process considered here. In particular, we give the cross section of the first charge exchange as a function of the $\bar{p}$'s speed, the distribution of binding energy of the resulting exotic atom and the distribution of angular momentum for the bound states. For the second stage, we give the binding energy distribution and the distribution of magnetic moments of the resulting atoms. But most importantly, we present results on the velocity distribution of resulting $\bar{H}$ atoms.

[1] The positron plasma and the $\bar{p}$ are assumed to be nearly pure because contamination with matter could substantially change the probabilities for the charge exchanges. For example, if the $\bar{p}$ plasma contains a substantial fraction of electrons, then $\bar{p}Cs^+$ plus an electron could lead to a charge exchange back to Cs^* plus a free $\bar{p}$. The positron plasma could be contaminated with positive ions.

As in [13], we will use a classical trajectory Monte Carlo (CTMC) method to compute the properties of the $\bar{p}Cs^+$ and $\bar{H}$. This should be an accurate method because the states that are involved have large quantum numbers: for example, $n \sim 50$. To simplify the discussions, we will assume that the magnetic field and the initial atom beam are in the z-direction.

2. Computational method

In this section, we describe aspects of how we solve the classical equations, the approximation used for the forces and how we generate the distributions needed for the random nature of the two charge transfer processes.

2.1. Numerical solution of classical equations

The main approximation was to use classical mechanics for the motion of all particles. The classical approximation should be accurate because we will be using Rydberg states with a large n (n is approximately 50 in Cs and $\bar{H}$ and approximately 2000 in $\bar{p}Cs^+$). Typically, the correspondence principle works well for highly excited atomic states unless the process is classically forbidden (for example, by energy or phase space restrictions) or if the process involves going from one small region of phase space to another small region (of order $\sim \hbar$). The processes considered in this paper are classically allowed and all of our results involve substantial averaging over initial conditions (i.e. large regions of phase space) which tends to remove any changes due to interference over different paths.

In our numerical simulation, we utilized the adaptive step size, fourth-order Runge–Kutta time propagation scheme [14], to numerically solve the classical equations of motion. We chose the accuracy parameter small enough so that only a small percentage of trajectories had unacceptable error but large enough so that we could run enough trajectories needed for good statistics. We checked the accuracy of each trajectory by comparing conserved quantities (e.g. total energy) at the end of the trajectory to that at the beginning. Any trajectory with a change in a conserved quantity larger than 0.1% was rejected from our sample. Our rejection rate was very low and should not affect our results; for example, only 0.01–0.03% of the trajectories that gave a charge exchange were rejected for $n = 50$ at $B = 1$ T. We used the full equations of motion for the electron, positron and $\bar{p}$ since it was not clear how accurate various approximations (e.g. the guiding centre approximation) would be for all of the fields and energies in our calculations. However, the Cs^+ ion was taken to have an infinite mass; since the ion's mass is more than $100\times$ that of the next heaviest particle and it moves along the B-field, this approximation should give errors less than 1% which is larger than the uncertainty from the Monte Carlo statistics. In all calculations, the Cs^+ is taken to be fixed in space (i.e. the calculations are in the frame of the Cs^+).

We approximated the interaction of the Cs^+ ion with all particles as being a pure Coulomb force for all distances. This is clearly a poor approximation when either the e^- or $\bar{p}$ is within $\sim 10^{-10}$ m of the nucleus. However, the number of trajectories that traverse this region is small for the highly excited states used in practice and all of the interesting physics occurs when the particles are far from the nucleus. Thus, we expect this approximation to be very good for the results reported below.

We also neglect the possibility of annihilation while the $\bar{p}Cs^+$ travels to the e^+ plasma. However, this will only be a small fraction of the atoms formed because the $\bar{p}Cs^+$ are in very high angular momentum states and thus, the $\bar{p}$ do not penetrate the core region. The angular momentum distribution will be given below and for Cs^* in $n = 50$ gives a spread up to $L \sim 2500\ \hbar$. Thus, direct annihilation due to Stark mixing into $L = 0$ will at most affect $\sim 1/2500$ atoms. Radiative cascade from these high states of $\bar{p}Cs^+$ is also negligible because the radiative lifetimes to decay to tightly bound states is longer than 1 s and the time to travel between plasmas will likely be less than 1 ms.

2.2. Initial distributions

It seems likely that if this scheme is tried experimentally then the Cs atom will be excited to the Rydberg state just before reaching the $\bar{p}$ plasma; the examples in this paper are for $n = 50$ states of the Cs atom. Typically, this is done with one or two photons from a low lying state; a possible sequence would be to excite the atom from the 5s to a 5p state and then excite the 5p state to a Rydberg state. Because few photons are involved, this means the Rydberg state will have low angular momentum in the z-direction (the magnetic field is assumed to be in the z-direction). To mimic this effect, the Rydberg electron is launched from a random point on a sphere with a radius of 1 nm with a random direction of the initial velocity. The initial speed of the electron is chosen so that the energy of the classical atom exactly matches that of an $n = 50$ state in hydrogen.

A strong magnetic field on a high Rydberg state causes a precession of the orbit. To allow for the precession to occur and reach a random point in the ensemble, each $\bar{p}$ is launched a large distance from the atom so that there are approximately 1000 Rydberg periods while the $\bar{p}$ travels to the atom. To ensure that the $\bar{p}$ does not always arrive at the atom after the same time, the launch distance is chosen randomly from a range of distances. The initial xy position of the $\bar{p}$ was chosen randomly from a square with the range $-3r_{Cs} \leqslant (x, y) \leqslant 3r_{Cs}$ where r_{Cs} is the size of the Rydberg state, $2\ n^2\ a_0$ with $n = 50$; the range of x, y is chosen to be large enough so transitions occur only in this range but not so large that we are calculating a large fraction of trajectories with no transfer. Convergence with respect to the range of (x, y) and the initial z was checked by increasing the values for all velocities.

After each $\bar{p}$ is launched, that run continues until either the $\bar{p}$ or the electron reaches the $\bar{p}$'s initial distance from the atom in the z-direction. When this occurs, that run is stopped. If the particle that reaches this position is an electron, the position and velocity vectors of the $\bar{p}$ is saved to a file to be used as input in the second charge exchange. The charge transfer cross section is the fraction of trajectories that give a bound $\bar{p}$ times the (x, y) area that they are launched through: $(2 \times 3r_{Cs})^2$.

In our second charge exchange, we simulated the formation of $\bar{H}$ by having the highly excited $\bar{p}Cs^+$ calculated

from the first stage interact with a thermal distribution of e^+'s. To ensure the $\bar{p}Cs^+$ was not preferentially oriented, we propagated this exotic atom for a random time with a flat distribution between 0 and 2000 Rydberg periods of the exotic atom to somewhat randomize the position of the $\bar{p}$. In an experiment, the $\bar{p}Cs^+$ will traverse regions of relatively strong electric fields (not strong enough to strip but strong enough to cause substantial angular momentum and Runge Lenz vector precession). This effect of E-fields is impossible to determine without simulation of an actual apparatus. Since the atoms will be nearly on the axis, the E-field will be mainly along the z-direction which means the z-component of $\vec{L}$ and the Runge–Lenz vector will not change; since the z-components of these vectors are proportional to the magnetic and electric dipole moments respectively, the distribution of internal parameters for the $\bar{p}Cs^+$ is likely to be qualitatively unchanged.

Each positron was given a random velocity from a thermal distribution. The perpendicular components v_x, v_y were given a Gaussian distribution proportional to $\exp(-mv^2/2k_BT)$ while the v_z distribution is proportional to $v\exp(-mv^2/2k_BT)$ (the extra power of v accounts for the speed in the calculation of the rate, $\langle v\sigma\rangle$). The positrons were launched a distance from the atom of $50r_{Cs}$ in the z-direction, and the initial xy position was chosen randomly from a square with the range $-3r_{Cs} \leqslant (x, y) \leqslant 3r_{Cs}$. This system was propagated until either the positron or $\bar{p}$ reached a distance of $60r_{Cs}$ from the Cs^+ ion. If the positron and $\bar{p}$ were within $3r_{Cs}$ of each other, their positions and velocities were saved for the last stage of the calculation.

In the last stage, the output from the second charge transfer is used to propagate the equations of motion until either the positron or $\bar{p}$ reached a distance of $140r_{Cs}$ from the Cs^+ ion. If the positron and $\bar{p}$ were within $3r_{Cs}$ of each other, then they have formed an $\bar{H}$ atom. From this $\bar{H}$ atom, the positions and velocities are used to compute the centre of mass velocity, the binding energy and the magnetic moment of the atom. Actually, this final calculation is not straightforward because of the strong magnetic field. The average centre of mass velocity is computed by taking the difference in position from the beginning of this stage to the end of the stage and dividing by the elapsed time. The internal energy is taken to be the total energy minus the kinetic energy computed from the average centre of mass velocity. Finally, the magnetic moment can be obtained by computing the time average of the quantity $m(xv_y - yv_x)$ with the positions and velocities being from the relative coordinates of the positron from the $\bar{p}$.

3. Results

We computed statistics associated with the physical properties of the composite particles. Calculations were performed for a specific initial principle quantum number: $n = 50$ and for 1, 2 and 4 T magnetic fields. Many, but not all, of the results can be scaled with n. For example, cross sections tend to scale like n^4 in 0 field. To get perfect scaling, n and B would need to be simultaneously changed. These values were chosen since they are probably near the values that would be chosen experimentally. Only for the 1 T case we have performed a
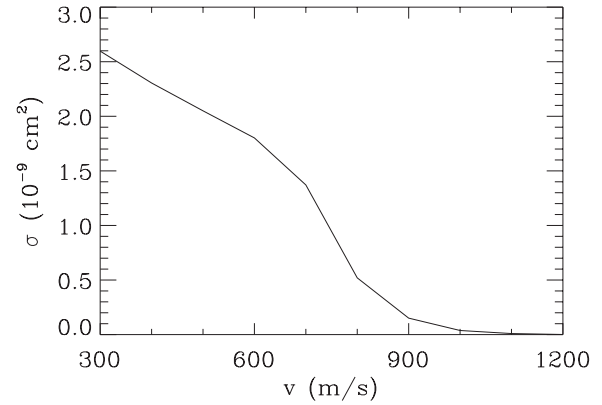

Figure 2. The cross section for the charge transfer formation of $\bar{p}Cs^+$. The $\bar{p}$ has a velocity v in the direction of the magnetic field (1 T) and the Cs atom is in a low angular momentum state with a binding energy corresponding to $n = 50$ of hydrogen. The cross section shown is only for $\bar{p}Cs^+$ with binding energy greater than 13.6 eV/65^2.

fine scale calculation in the the initial speed of the $\bar{p}$: steps of 100 m s^{-1} between 300 and 1200 m s^{-1}. For the other magnetic fields, the initial speeds were chosen to be 500, 700 and 900 m s^{-1} which bracket the likely experimental values.

3.1. $\bar{p}Cs^+$ properties

For the first charge transfer, we transform to the frame of the Cs^+. The $\bar{p}$'s will have a distribution of velocities. We note that a $\bar{p}$ with a speed of 300 m s^{-1} has a kinetic energy of 5.4 K. Thus, a very cold $\bar{p}$ plasma could have average speeds much less than the speed of the Cs^+. Thus, the initial $\bar{p}$ speed in this section is roughly the speed of the Cs^+ ion once we have transformed to the Cs^+ frame. Calculation at 2 T gave very similar distributions to the ones given below; the overall cross section was approximately 30% higher for 2 T at 500 and 700 m s^{-1} and approximately a factor of 2 larger at 900 m s^{-1}.

3.1.1. Cross section. The cross section for the charge transfer formation of $\bar{p}Cs^+$ with binding energy greater than that of an $n = 65$ state in H (i.e. 37 K) is shown in figure 2. We have chosen to limit the final states in the calculation to mimic the effect of an electric field; the electric fields in the traps will strip the $\bar{p}$ from the Cs^+ if the binding energy is too small. By choosing the binding energy to be greater than ∼37 K, we are restricting the $\bar{p}Cs^+$ to states that would survive electric fields of ∼20 V cm^{-1}. The cross section is shown as a function of the initial speed of the $\bar{p}$ which is assumed to be travelling in the z-direction. A 1 T magnetic field is in the z-direction. As a point of comparison, the geometrical size of the original $n = 50$ Cs atom is 0.26 μm which gives a geometrical area $\pi r^2 \simeq 2.2 \times 10^{-9}$ cm^2.

The cross section is somewhat larger than geometrical at the lowest velocity and rapidly decreases over the velocity range from 600 to 900 m s^{-1}. By 1200 m s^{-1}, the cross section has become more than two orders of magnitude smaller than geometric. The rough sizes involved in figure 2 can be understood by relatively simple arguments.
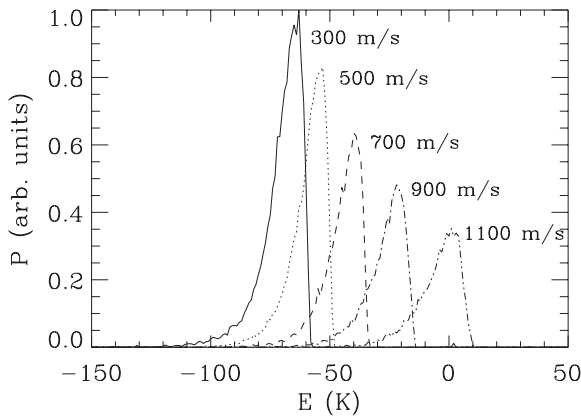
Figure 3. The distribution, P, of internal energies of the p̄Cs⁺ formed in the first charge transfer. These are for all trajectories where the electron reaches the final distance before the p̄. The distributions are for the same starting parameters as in figure 2. The different lines are for an initial p̄ speed of 300 (solid), 500 (dotted), 700 (dashed), 900 (dot-dashed) and 1100 m s^{-1} (dot-dot-dot-dashed). All distributions have been normalized by the same factor so the relative size is real.

Figure 4. The distribution, P, of perpendicular angular momentum, $L_\perp = \sqrt{L_x^2 + L_y^2}$, of the p̄Cs⁺ formed in the first charge transfer. This distribution is only for p̄Cs⁺ with binding energy greater than 13.6 eV/65^2. The same conditions and line types as in figure 3 hold. The sharp decrease in size for 900 and 1100 m s^{-1} data is due to most atoms being bound by less than 13.6 eV/65^2. Note that the distributions extend to the highest allowed values.

At low velocities, the size is roughly geometrical because the p̄ is heavy so that the deflection of the trajectory is not large if it has an impact parameter more than ∼2× the atomic size. Because the p̄ and electron have the same charge, the electron gets pushed to the other side of the atom and then it is ionized as the p̄ approaches the atom. By energy conservation, the p̄ must be bound after the atom is ionized if the p̄ starts at low kinetic energy compared to the original binding energy of the Cs atom. At low initial kinetic energies, the p̄ can only be captured into orbits with a size smaller than the original size of the atom.

The sharp drop in cross section with velocity can be understood from conservation of energy. When the electron leaves the atom, it is most likely to carry away little energy because the p̄ approaches slowly. Thus, the binding energy of the p̄Cs⁺ will peak at the original binding energy of the Cs minus the original kinetic energy of the p̄; this will be shown in the next section. In figure 2, we show the cross section to states with binding energy greater than 13.6 eV/65^2. A p̄ with a kinetic energy corresponding to the difference in energy between $n = 50$ and 65 gives a speed of 650 m s^{-1}. Above this speed, the peak of the p̄Cs⁺ energy distribution is above the $n = 65$ cut-off energy.

3.1.2. Internal energy distribution. Figure 3 shows the distribution of internal energies of the p̄Cs⁺ formed in the first charge transfer. This distribution is for all trajectories where an electron reached the maximum distance before the p̄. Negative energies correspond to bound p̄Cs⁺ and positive energies correspond to unbound p̄'s. The parameters are the same as in the previous section. The distribution resulted for 220 000 trajectories run for each of the initial p̄ shown. All distributions have been normalized by the same factor.

There are a couple of important features to note. The most obvious is that the peak of the distribution shifts to higher energies as p̄ velocity increases. This is simply due to energy

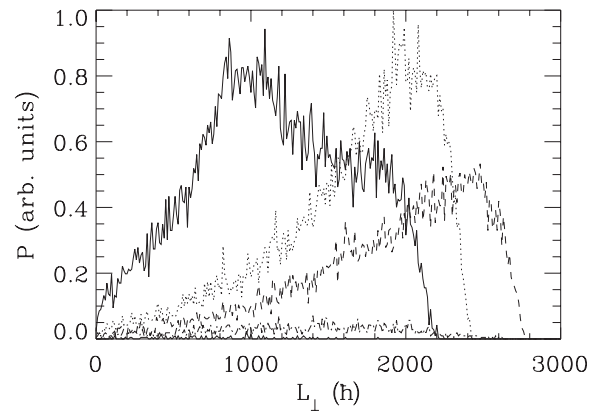conservation. The electrons tend to escape with relatively little kinetic energy so the peak of the distribution is at the total energy of the system: the original energy of the Cs atom (−13.6 eV/50^2 ≃ −63 K) plus the original kinetic energy of the p̄.

Another obvious feature is that the distribution has a spread. Since all trajectories start with the same total energy, this spread reflects the spread in the energy distribution of the escaping electron. This spread does not substantially change with the speed of the incident p̄ and is approximately 10–20 K.

A final obvious feature is that the overall size of the distribution decreases with increasing p̄ speed. This reflects the fact that fewer Cs ionizations occur with increasing speed. This is mostly due to the fact that the p̄ is deflected less at the higher speeds; at lower speeds, the p̄ trajectory can be bent due to the interaction with the induced dipole moment in the Cs atom. For favourable geometry, the p̄ can be pulled into the atom which increases the probability for charge exchange. There is some contribution to this trend due to the decrease in interaction time, but it is not the main effect. However, note that the decrease in distribution is much more gradual than the decrease in cross section which is mainly reflecting the fact that the distribution is shifting to higher energy.

3.1.3. Angular momentum distributions. Figures 4 and 5 show the angular momentum distributions for p̄Cs⁺ that form with a binding energy greater than 13.6 eV/65^2; these are the trajectories that count in the charge exchange cross section of figure 2. Figure 4 is the distribution of perpendicular angular momenta $\left(\sqrt{L_x^2 + L_y^2}\right)$ and figure 5 is parallel angular momentum (L_z). For these figures, the angular momenta do not include the vector potential from the B-field (e.g. $L_x = M(yv_z − zv_y)$) since the magnetic forces are weak for p̄Cs⁺. These angular momenta are not conserved quantities and so the distributions vary with time. These figures are for just after the p̄Cs⁺ has
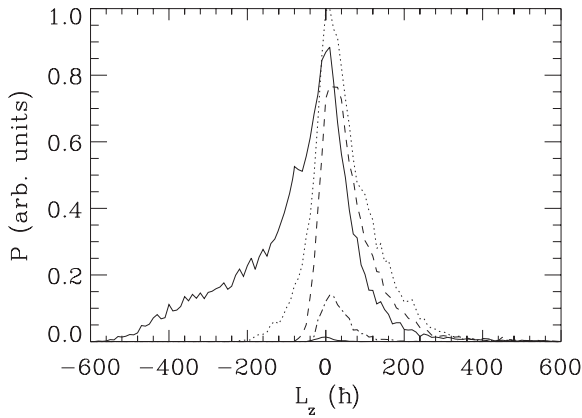
Figure 5. The distribution, P, of parallel angular momentum, L_z, of the $\bar{p}Cs^+$ formed in the first charge transfer. Note this distribution is much narrower than that in figure 4 which indicates that the angular momentum is approximately perpendicular to the original velocity of the $\bar{p}$.

formed and give some insight into the type of trajectories that give the bound states.

The very rapid drop in size of the distribution with increasing speed matches the drop in cross section shown in figure 2. Remember this is due to only accepting trajectories with sufficient binding energy.

Figure 4 shows that the perpendicular angular momenta extend up to the largest value allowed by energy conservation. In comparing figures 4 and 5, note that the much smaller scale for figure 5 means that the component of $\vec{L}$ along the direction of the original velocity vector of the $\bar{p}$ is relatively small. Remember, the largest angular momentum is for circular states which shows that the $\bar{p}Cs^+$ tends to form in nearly circular states with the normal to the plane of the orbit being perpendicular to the original $\bar{p}$ velocity.

The 300 m s^{-1} distribution clearly differs from those at 500 and 700 m s^{-1}. This is because the lowest $\bar{p}$ speed allows for trajectories to be bent while traveling to the Cs Rydberg atom. Thus, the trajectory as it approaches the atom tends to be more directly towards the atom which shows up as more population at smaller $L_\perp$. The L_z has a larger spread for the smallest velocity for a similar reason. The 300 m s^{-1} trajectories have substantially larger $v_\perp = \sqrt{v_x^2 + v_y^2}$ just before the $\bar{p}$ reaches the atom. Since L_z depends on v_x, v_y, the spread is broader for the lowest speed which is somewhat counterintuitive.

One interesting feature is that the distribution of $|\vec{L}|$ is very similar to that in figure 4 since the L_z distribution is narrow. For the 500 and 700 m s^{-1} distributions, the distribution increases approximately linearly until the maximum value of $|\vec{L}|$. If the atoms had a microcanonical ensemble of trajectories, then the $|\vec{L}|$ distribution would have this shape *and* have a random direction for $\vec{L}$. Since the distribution after the charge exchange does not have a random direction for $\vec{L}$, the distribution is not microcanonical. However, if there were some feature of the experiment that scrambled the direction of $\vec{L}$ after the charge transfer then the distribution would be a good approximation to microcanonical.

In figure 4, the shape of the distribution for 900 and 1100 m s^{-1} is not clearly shown due to the small size of the cross section. Although the statistics for these calculations is not great, there is a clear change in shape from the 500 and 700 m s^{-1} distributions. The distribution for 900 m s^{-1} peaks for $L_\perp \sim 1500\hbar$ while the distribution for 1100 m s^{-1} peaks for $L_\perp \sim 1000\hbar$. This is another somewhat counterintuitve result: higher speed for the $\bar{p}$ results in smaller angular momentum. The reason for the change at the higher speeds is that the electron must leave with substantial kinetic energy if the binding energy of the $\bar{p}Cs^+$ is to be greater than 13.6 eV/65^2. For the electron to leave with relatively high energy, an especially close interaction between the $\bar{p}$ and electron must occur. This argues for a more direct 'hit' on the atom and thus a lower angular momentum.

3.2. $\bar{H}$ properties

Calculations for the second charge transfer are also performed in the frame of the Cs$^+$ ion. The second charge transfer occurs when a positron hits the Rydberg $\bar{p}Cs^+$ and converts to a Rydberg $\bar{H}$ and a Cs$^+$ ion. We used the distribution of Rydberg $\bar{p}Cs^+$ from the previous section (with the $n = 65$ cutoff) as the starting point. The positrons that interact with the $\bar{p}Cs^+$ will have average speeds more than an order of magnitude larger than the speed of the $\bar{p}Cs^+$. Thus, the positrons are launched with an unshifted thermal distribution. For 1 T fields, we performed the second charge transfer calculation at 4, 8 and 12 K. The distributions did not change substantially, but the transfer rate decreased by a factor of 0.7 from 4 to 12 K.

In all of the figures, the distributions of the $\bar{H}$ properties for the different initial Cs* speeds do not include the smaller probability of $\bar{p}Cs^+$ formation as v_z increases. The distributions are normalized so that the same number of $\bar{H}$'s are formed for each v_z. Thus, absolute numbers of $\bar{H}$'s formed in a given range would need to be multiplied by the cross section of figure 2 and charge transfer rate given below.

3.2.1. Charge transfer rate. The rate for the reaction is an important quantity because it determines the density and length of the e$^+$ plasma needed for effective formation of $\bar{H}$'s. We can compute the rate from

$$\langle v\sigma \rangle = f \cdot A \cdot \sqrt{k_B T/m}, \tag{1}$$

where A is the area through which we fire the e$^+$, f is the fraction of e$^+$ that led to charge transfer, T is the e$^+$ temperature and m is the e$^+$ mass. We performed calculations for low temperature e$^+$: 4, 8 and 12 K. For $B = 1$ T and 4 K, the factor $f \cdot A \simeq 0.78(2n^2a_0)^2 \simeq 5.5 \times 10^{-10}$ cm^2 which gives a rate of $\simeq 4.3 \times 10^{-4}$ cm^3 s^{-1}. Thus, if the $\bar{p}Cs^+$ is in an e$^+$ plasma of 10^8 cm^{-3}, the lifetime for a transfer is roughly 24 μs and the path length for a transfer is 1.2 cm if it is travelling at 500 m s^{-1}. At 8 K, the factor $f \cdot A \simeq 0.47(2n^2a_0)^2 \simeq 3.3 \times 10^{-10}$ cm^2 which gives a rate of $\simeq 3.6 \times 10^{-4}$ cm^3 s^{-1}. At 12 K, the factor $f \cdot A \simeq 0.31(2n^2a_0)^2 \simeq 2.2 \times 10^{-10}$ cm^2 which gives a rate of $\simeq 3.0 \times 10^{-4}$ cm^3 s^{-1}.
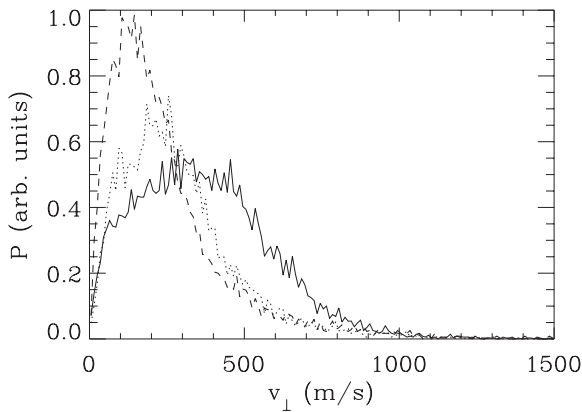
Figure 6. The distribution, P, of the perpendicular velocity of $\bar{H}$ formed in the second charge transfer. The distributions are for the same starting parameters as in figure 2 and for a positron plasma at 4 K. The different lines are for an initial $\bar{p}$ speed of 500 (solid), 700 (dotted) and 900 (dashed). In figures 6–9, the distributions of the $\bar{H}$ properties for the different initial Cs* speeds do not include the smaller probability of $\bar{p}Cs^+$ formation as v_z increases. The distributions are normalized so that the same number of $\bar{H}$'s are formed for each v_z.
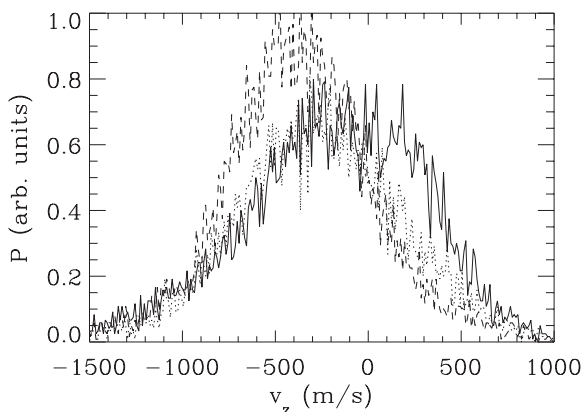

Figure 7. The distribution, P, of the parallel velocity of $\bar{H}$ formed in the second charge transfer. The distributions are for the same starting parameters as in figure 6.

3.2.2. Velocity distribution. Figures 6 and 7 show the perpendicular and parallel velocity distribution in the frame of the Cs$^+$ for $\bar{H}$ formed in a 1 T magnetic field and in a 4 K e$^+$ plasma. The solid line is when the original Cs Rydberg atom travelled at 500 m s^{-1}, while the dotted line is 700 m s^{-1} and the dashed line is 900 m s^{-1}. The distributions have been normalized by the same factor; thus, the relative sizes show actual differences.

Figure 6 shows two important features. The first is that the width of the perpendicular velocity distribution becomes smaller as the initial speed of the Cs Rydberg atom is increased. This is partly due to the fact that the binding energy of the $\bar{p}Cs^+$ decreases with increased energy of the initial Rydberg atom, see figure 3. But it is also due to the plane of the orbit giving $\vec{L}$ of the $\bar{p}Cs^+$ being more strongly perpendicular to the z-direction.

The second important feature is the size scale. Note that an $\bar{H}$ travelling at 100 m s^{-1} has a kinetic energy of 0.61 K,

200 m s^{-1} has 2.4 K and 300 m s^{-1} has 5.4 K. Typical magnetic trap depths proposed for $\bar{H}$ in the ground state is in the 1/2 to 1 K range. Thus, most atoms in figure 6 have too much kinetic energy. However, the mechanism discussed in [15, 16] can provide substantial cooling in the perpendicular direction. The perpendicular kinetic energy can be substantially cooled if the atoms enter a region where there is a multipole field which increases in magnitude as the atoms move away from the trap axis. As will be seen below, a substantial fraction of the atoms have a large initial magnetic moment which is the precondition for this cooling. Overall, the data shown in figure 6 is a positive feature.

Figure 7 shows the parallel velocity distribution and also shows two important features. The first greatly surprised us. In the frame of the Cs$^+$ ion, the $\bar{H}$ atoms are preferentially emitted with negative v_z instead of with an $\langle v_z \rangle \sim 0$ as we expected. Since the original $\bar{p}$'s were given positive velocity in the Cs$^+$ frame, the lab frame velocity of the Cs$^+$ is negative and thus the $\bar{H}$ are preferentially emitted in the direction of the original Cs atom's motion. After the first charge transfer, the time average of v_z for the $\bar{p}$ attached to the Cs$^+$ must be 0 in the frame of the Cs$^+$. However, the $\bar{p}Cs^+$ has a non-zero, time-averaged electric dipole moment. In our calculations, we found that the $\langle z \rangle$ for 500 m s^{-1} was -0.3 r_{Cs}, -0.6 r_{Cs} for 700 m s^{-1} and -0.8 r_{Cs} for 900 m s^{-1}. The $\bar{p}Cs^+$ has a non-zero, time-averaged electric dipole moment *because* the original Rydberg Cs* has a large, non-zero velocity in the z-direction which corresponds to a velocity distribution for $\bar{p}$'s in the Cs* frame being centred at $-v_z$ and not at $\vec{v} = 0$: the initial conditions of the formation are not the same for $z \rightarrow -z$. For weak electric and magnetic forces in the z-direction, the Runge–Lenz vector and the angular momentum vectors precess about the z-axis which means their z-components are conserved. Since the Runge–Lenz vector is proportional to the electric dipole moment, the z-component of the dipole moment just after formation is conserved.

During the second recombination the $\bar{H}$ interaction with the Cs$^+$ gives it a velocity along this direction. So it seems that the recombination process causes the $\bar{H}$ to recoil along the direction of $\langle z \rangle$. This seems reasonable in that the $\bar{H}$ does not need to pass by the Cs$^+$ atom in this case.

The second important feature is the width of the distribution. Unfortunately, the full width at half maximum is approximately 700–800 m s^{-1}. Thus, while we can talk about a beam of $\bar{H}$, the velocity spread could be too large to be useful. There are a couple of possibilities for obtaining a narrower distribution discussed below. The large width of the velocity was a surprise to us. The root mean square speed for a $\bar{p}$ corresponding to a binding energy of 13.6 eV/60^2 is approximately 850 m s^{-1}. We expected the spread for $\bar{H}$ to be much less than this because the v_z is only one component of the speed so we expected the spread in figure 7 to be reduced from 850 m s^{-1} by a factor of between $\sqrt{2}$ and $\sqrt{3}$. We also expected the recombination to mainly occur when the $\bar{p}$ was near its outer turning point where its speed is a minimum because the positron is repelled by the Cs$^+$ ion. These expected reductions did not occur.

Although the spread in the velocity distribution was larger than we expected, it could be that this is still a competitive
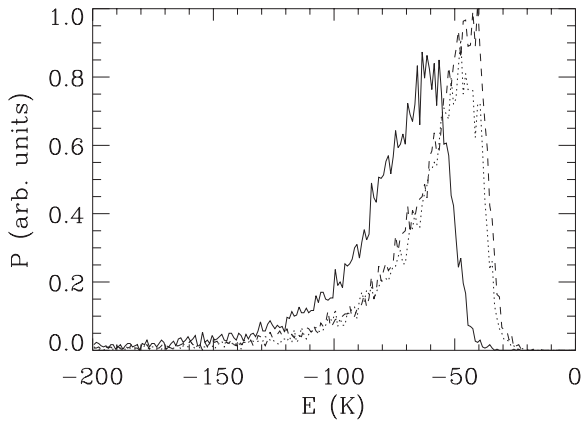
Figure 8. The distribution, P, of the internal energy of H̄ formed in the second charge transfer. The distributions are for the same starting parameters as in figure 6. To orient the scale, $n = 50$ has a binding energy of 63 K and $n = 60$ a binding energy of 44 K.

Figure 9. The distribution, P, of the time average angular momentum, $L_z = \langle m(xv_y - yv_x) \rangle$, of H̄ formed in the second charge transfer. This quantity is proportional to the magnetic moment of H̄. The distributions are for the same starting parameters as in figure 6. Positive values of L_z correspond to atoms that are attracted to high magnetic fields. Thus, the negative L_z part of the distribution are the atoms that can be magnetically trapped. Atoms with large negative L_z can cool during a radiative cascade.

method for making cold H̄ compared to the current methods. One of the standard methods for forming H̄ is to have p̄'s pass through a positron plasma. With this standard method, the best scenario is when the p̄ come into thermal equilibrium with the positrons before forming a H̄. Also in the standard method, the positron plasma (and the p̄'s while inside) rotate about the trap axis with a rate proportional to the density and this rotational energy can lead to hot H̄. For the double charge exchange, the H̄ distribution mostly depends on the binding energy of the original Cs*.

3.2.3. Internal energy distribution. Figure 8 shows the distribution of internal energy of the H̄ atom. For the lower speed, the peak of the distribution is near the initial energy of the Cs atom. For the higher speeds the distribution shifts up in energy which reflects the lessened binding energy of the p̄Cs+ as discussed above. Thus, the initial binding energy of the Cs atom strongly determines the final binding energy of the H̄.

3.2.4. Angular momentum distribution. In a magnetic field, the magnetic moment is proportional to the time average of $m(xv_y - yv_x)$; positive values correspond to atoms attracted to high B while negative values correspond to atoms attracted to low B. For simplicity, we will call this quantity the angular momentum although it is *not* the canonical angular momentum that is conserved in a uniform B-field. Figure 9 shows the distribution of the time average of this quantity. One important feature is that the distribution is not symmetrical. This was seen in other calculations of recombination in a strong magnetic field (e.g. see [13]). Although most of the atoms are high field seeking in character, there is a substantial fraction of atoms with a very large magnitude magnetic moment *and* attracted to low B. These atoms experience a much deeper magnetic well depth. Furthermore, these atoms can cool the centre of mass kinetic energy during the radiative cascade [15, 16].
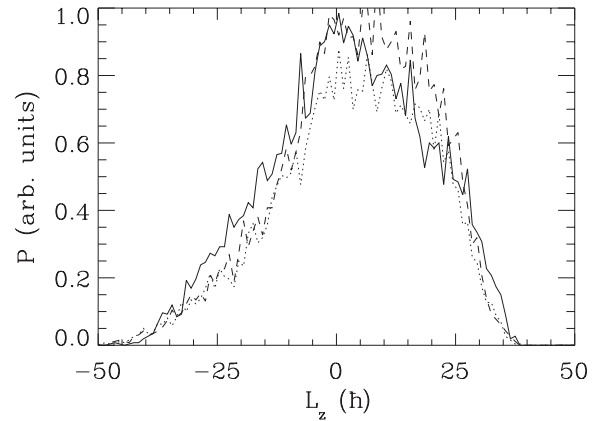
3.2.5. Fixing the velocity distribution. The z velocity distribution is wider than we originally hoped. But this is partly due to the choice for the initial state of the atom and the choice of the cut-off for the binding energy of p̄Cs+. These choices were made because the plasmas will need to be held in space by static electric fields which can strip the atoms. If weaker electric fields are used, then more weakly bound states will survive the travel between plasmas and would contribute to a narrower velocity spread.

Another possible fix is to use a method similar to that discussed in [17]. In this paper, a magnetic well moves with the atoms. Since the H̄ are initially in Rydberg states with large magnetic moments, a large fraction of the atoms will cool in the frame of the moving well as they radiatively cascade to the ground state. This method could substantially narrow the velocity distribution in a region near the maximum.

Finally, it is not completely clear how these calculated velocity distributions will match those seen in experiments. The reason is that electric fields in an experiment will tend to scramble the angular momentum and Runge–Lenz vector of the p̄Cs+. Since the recoiling velocity of the H̄ depends on the position and velocity of the p̄ inside of the exotic atom, these electric fields could change the velocity distribution. It seems likely that these changes would lead to a decreased spread in velocity since the current spread is roughly the maximum expected for these initial states.

3.3. Larger B-field

The calculations at higher magnetic fields are more intensive because the cyclotron motion causes the time steps in the classical propagator to decrease in size. Because the magnetic field most strongly affects the motion of low energy electrons and positrons, we repeated the calculations for the 500, 700 and 900 m s^{-1} Cs speeds in a 2 T field and for 4 K e+ plasma. Surprisingly, there was relatively little change in the parameters.

For the 2 T case, the cross section for the first charge transfer is a factor of 1.3 larger at 500 and 700 m s^{-1} and is a factor of 2.5 larger at 900 m s^{-1}. The large factor at 900 m s^{-1} is due to the fact that the cross section is small at that speed. The rate for the second stage transfer decreased by a factor of 0.83 for all speeds. Thus, the rates do not substantially change except for one case where the process is strongly suppressed.

We compared all of the distributions to the 4 K calculations at 1 T. While all distributions showed some differences, the changes were minor except for one parameter. Only the distribution of angular momentum of the H̄, figure 9, changed. The width of the distribution for $B = 2$ T was approximately a factor of 0.6 times that for 1 T. This is probably due to the smaller cyclotron orbit in the large B-field. The smaller width will reduce the fraction of H̄ with very large magnetic moments which could reduce the cooling during the radiative cascade.

4. Other processes

It should be noted that there are some processes that have not been included in the simulations. First, we have not included three-body recombination: two e$^+$ scatter in the field of the Rydberg p̄Cs$^+$ leading to a Rydberg H̄. If this process occurs, it is likely to be with a rate somewhat reduced from the simple three-body recombination to a bare p̄. The reason being that the Cs$^+$ ion will tend to repel e$^+$'s. However, if it occurs, it seems like it should most likely occur when the p̄ is at its furthest distance from the Cs$^+$. In this case, the resulting H̄ may have a much smaller spread of velocities than for the process discussed in this paper. This effect could become comparable to that calculated in this paper for high density e$^+$ plasma (greater than 10^8 cm^{-3}) and low temperatures (4 K).

Second, we have not included further charge transfer and inelastic collisions between H̄'s and e$^+$ that can occur once the second charge exchange has occurred. This process will have a rate several times geometric. Thus, it will probably occur to some extent. However, the result is H̄ with almost the same centre of mass velocity as before the collision. The collisions will tend to randomize the angular momentum and increase the binding energy of the H̄ unless the e$^+$ temperature is comparable to the binding energy. Thus, the results presented in the previous section should not be substantially changed by this collision process.

5. Conclusions

We have simulated the formation of H̄ through a two-stage charge exchange mechanism. This mechanism can be used to efficiently generate cold H̄ without having the plasmas at the coldest possible temperatures; for example, temperatures of ∼20 K would be sufficient compared to the ∼4 K temperatures which is the goal of current experiments. The temperature of the resulting H̄ most strongly depends on the initial binding energy of the Cs* atom; in the example in this paper, the kinetic energy of the H̄ was ∼15 K compared to the 63 K binding energy of the Cs*. This process could also be used to generate an H̄ beam although the velocity spread along the beam direction is calculated to be wider than we expected; we expected the velocity spread to be substantially smaller than that for the p̄ in the p̄Cs$^+$ atom. By pulsing the Rydberg Cs (e.g. by using a pulsed laser to excite to the atom), the time when the H̄ forms can be controlled at the ∼10 μs level could be useful in reducing background during measurements.

References

[1] Amoretti M *et al* (ATHENA Collaboration) 2002 *Nature* **419** 456
[2] Gabrielse G *et al* (ATRAP Collaboration) 2002 *Phys. Rev. Lett.* **89** 213401
[3] Andresen G B *et al* (ALPHA Collaboration) 2008 *Phys. Rev. Lett.* **100** 203401
[4] Gabrielse G, Rolston S L, Haarsma L and Kells W 1988 *Phys. Lett.* A **129** 38
[5] Glinsky M E and O'Neil T M 1991 *Phys. Fluids* B **3** 1279
[6] Robicheaux F and Hanson J D 2004 *Phys. Rev.* A **69** 010701
[7] Kellerbauer A *et al* 2008 *Nucl. Instrum. Methods Phys. Res.* B **266** 351
[8] Mohri A and Yamazaki Y 2003 *Europhys. Lett.* **63** 207
[9] Phillips T 2009 private communication
[10] Ordonez C A 2009 *J. App. Phys.* **106** 024905
[11] Hessels E A, Homan D M and Cavagnero M J 1998 *Phys. Rev.* A **57** 1668
[12] Storry C H *et al* 2004 *Phys. Rev. Lett.* **93** 263401
[13] Wall M L, Norton C S and Robicheaux F 2005 *Phys. Rev.* A **72** 052702
[14] Press W H, Teukolsky S A, Vetterling W T and Flannery B P 1992 *Numerical Recipes* 2nd edn (New York: Cambridge University Press))
[15] Taylor C L, Zhang Jingjing and Robicheaux F 2006 *J. Phys. B: At. Mol. Opt. Phys.* **39** 4945
[16] Pohl T, Sadeghpour H R, Nagata Y and Yamazaki Y 2006 *Phys. Rev. Lett.* **97** 213001
[17] Narevicius E, Parthey C G, Libson A, Riedel M F, Even U and Raizen M G 2007 *N. J. Phys.* **9** 96